CHEMISTRY OF MATERIALS

ARTICLE

pubs.acs.org/cm

Synthesis and Photoelectrochemical Properties of $Fe_2O_3/ZnFe_2O_4$ Composite Photoanodes for Use in Solar Water Oxidation

Kenneth J. McDonald and Kyoung-Shin Choi*

Department of Chemistry, Purdue University, West Lafayette, Indiana 47907, United States

Supporting Information

ABSTRACT: α-$Fe_2O_3/ZnFe_2O_4$ composite electrodes are prepared via a simple surface treatment performed on nanoparticulate α-Fe_2O_3 electrodes. The α-Fe_2O_3 electrodes are uniformly covered with a solution containing Zn^{2+} ions which react with Fe_2O_3 upon heating to form $ZnFe_2O_4$. As Zn^{2+} ions do not completely diffuse into the core of Fe_2O_3 particles under mild heating conditions, the $ZnFe_2O_4$ forms only on the surface of Fe_2O_3 as a shell layer, resulting in the formation of $Fe_2O_3/ZnFe_2O_4$ composite electrodes. Any unreacted ZnO is removed by dissolution in 1 M NaOH, where $ZnFe_2O_4$ and Fe_2O_3 are stable. X-ray diffraction and energy-dispersive spectroscopy studies show that a crystalline $ZnFe_2O_4$ phase forms after the heat treatment and the composite electrode with the best photoelectrochemical performances contains a 1:1 mol ratio of $ZnFe_2O_4$ and Fe_2O_3. The $Fe_2O_3/ZnFe_2O_4$ composite electrode shows a significantly enhanced photocurrent response compared to the bare Fe_2O_3 electrode because $ZnFe_2O_4$ has conduction and valence band edges shifted ca. 200 mV from those of Fe_2O_3 to the negative direction which allows for the efficient separation of electron−hole pairs at the $Fe_2O_3/ZnFe_2O_4$ interface. Further improvement in photocurrent is observed when the surface is modified by an Al^{3+} treatment that forms thin $ZnFe_{2-x}Al_xO_4$ or $Fe_{2-x}Al_xO_3$ layers that reduce surface states created by Fe^{3+} ions exposed on the surface having imperfect coordination environments. The formation of $ZnFe_2O_4$ and Al^{3+}-containing layers make the surface less catalytic for O_2 evolution, and therefore, introduction of the Co^{2+} ions as oxygen evolution catalysts further improved the over performance of the composite electrodes.

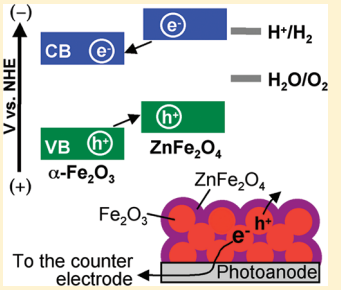

KEYWORDS: zinc ferrite ($ZnFe_2O_4$), iron oxide (Fe_2O_3), water oxidation, photoanode, solar energy conversion

1. INTRODUCTION

α-Fe_2O_3 is an n-type semiconductor that has many desirable properties for use as a photoanode in a photoelectrochemical cell used to photoelectrolyze water.[1−3] It has a band gap of 2.1 eV, which allows for utilizing a significant visible portion of the solar spectrum and a valence band edge position that allows for sufficient overpotential for the oxidation of water to O_2. Furthermore, it is environmentally benign, abundant, and capable of withstanding neutral and alkaline conditions. Many of the desired properties of Fe_2O_3 are shared with Fe-based ternary oxides classified as ferrites that have a chemical formula of MFe_2O_4 where M are divalent ions such as Zn^{2+}, Mg^{2+}, and Ca^{2+}.[4−12] In particular, n-type $ZnFe_2O_4$ is promising as a photoanode for photoelectrolysis of water because, while its band gap ($E_g \approx 2$ eV) is comparable to that of α-Fe_2O_3 and is also chemically and photochemically stable in basic media,[4,5] its conduction and valence band edges are shifted to the negative direction by ca. 200 mV, situating the conduction band edge very near the hydrogen evolution potential (Scheme 1a).[6] As a result, a photoelectrochemical cell based on n-type $ZnFe_2O_4$ as a photoanode will require a smaller external bias to split water than that required for a Fe_2O_3-based photoelectrochemical cell.

Compared to Fe_2O_3, ferrites have been far less studied as photoanodes for photoelectrochemical water splitting cells. It is most likely because it is less straightforward to produce high quality electrodes of ternary oxides than binary oxides. Previous research on $ZnFe_2O_4$ has mainly focused on using $ZnFe_2O_4$ as

Scheme 1. (a) Band Positions of α-Fe_2O_3 and $ZnFe_2O_4$ at pH 13.6 and (b) Schematic Representation of the Core−Shell Structure of a $Fe_2O_3/ZnFe_2O_4$ Electrode

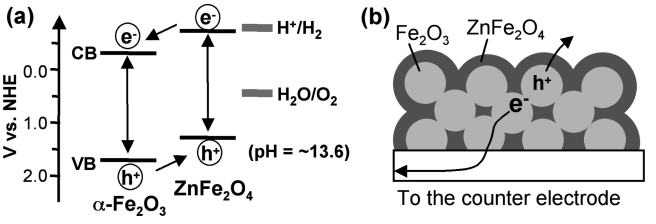

powder-type or colloidal photocatalysts for the decomposition of organics compounds.[13−18] Only a few studies report using $ZnFe_2O_4$ as a photoanode in a water photoelectrolysis cell with promising results in basic media.[4,5] Other photoelectrochemical studies of $ZnFe_2O_4$ involved pairing $ZnFe_2O_4$ with wide band gap materials such as TiO_2 to use $ZnFe_2O_4$ as a small band gap material to increase visible-light absorption.[19,20]

In this study, we prepared a $Fe_2O_3/ZnFe_2O_4$ composite electrode by converting the surface of nanoporous Fe_2O_3 to

Received: August 12, 2011
Revised: October 2, 2011
Published: October 17, 2011

$ZnFe_2O_4$ using a simple solution/heat treatment. Because the conduction and valence band edge positions of $ZnFe_2O_4$ are ideally offset from those of Fe_2O_3, we postulated that combining Fe_2O_3 and $ZnFe_2O_4$ can effectively enhance the separation of electron−hole pairs generated in both Fe_2O_3 and $ZnFe_2O_4$ regions by allowing movement of electrons and holes to the opposite direction (Scheme 1a). Because the valence band edge of $ZnFe_2O_4$ is located at a more negative potential than that of Fe_2O_3, an ideal architecture of the $Fe_2O_3/ZnFe_2O_4$ composite photoanode that could best utilize the band edge offset is $ZnFe_2O_4$ layers surrounding Fe_2O_3 cores as shown in Scheme 1b. In this configuration, the hole generated in the Fe_2O_3 region can be transferred to the $ZnFe_2O_4$ layer and then be consumed at the $ZnFe_2O_4$ /electrolyte junction which should be highly advantageous for harvesting more holes generated in Fe_2O_3 that is known to have an extremely short diffusion length.[21,22] The electrons generated in the $ZnFe_2O_4$ layer can move to the Fe_2O_3 cores and travel to the back contact.

Here, we report the synthesis, characterization, and photoelectrochemical properties of $Fe_2O_3/ZnFe_2O_4$ composite photoanodes for the photoelectrolysis of water having an architecture similar to that shown in Scheme 1b. We also modified the surface of the $Fe_2O_3/ZnFe_2O_4$ composite electrode with Al^{3+} ions and Co^{2+} ions to reduce surface states and enhance catalytic abilities, respectively, and investigated their effect on photocurrent generation. The simple solution/heat procedure reported here can be used as a general strategy to partially or fully convert binary oxide electrodes generated from various synthesis methods to produce photoelectrodes composed of ternary oxides.

2. EXPERIMENTAL SECTION

Electrochemical Synthesis of Nanoporous α-Fe_2O_3 Electrodes. Detailed deposition mechanism and method to prepare nanoporous α-Fe_2O_3 electrodes via electrodeposition and the complete characterization of the resulting electrodes can be found elsewhere.[2,3] Briefly, amorphous FeOOH films were anodically deposited at 75 °C using an aqueous solution containing 20 mM $FeCl_2 \cdot 5H_2O$ (ACS, 99+% purity, Aldrich). A standard three-electrode setup in an undivided cell was used. Fluorine-doped tin oxide (FTO) (sheet resistance ∼8−12 Ω, Hartford Glass Company) was used as the working electrode while a platinum electrode, which was prepared by sputter coating a 200 Å Ti layer followed by a 1000 Å Pt layer on cleaned glass substrates, was used as the counter electrode. The reference electrode was an Ag/AgCl electrode in 4 M KCl solution, against which all the potentials reported herein were measured. The films used in this study were deposited at +1.2 V for 14 min with average deposition current density of ca. 0.38 mA/cm^2. In order to obtain crystalline nanoporous α-Fe_2O_3 electrodes, as-deposited films were annealed in atmosphere at 520 °C for 6 h after a ramp rate of 2 °C/min.

Preparation of $Fe_2O_3/ZnFe_2O_4$ Composite Electrodes. $Fe_2O_3/ZnFe_2O_4$ composite electrodes were prepared by pipetting 75 μL aqueous solutions of 60 mM $Zn(NO_3)_2$ onto the nanoporous Fe_2O_3 electrodes. This volume was enough to completely cover Fe_2O_3 electrodes that have the dimensions of 1 cm ×1.75 cm × ca. 520 nm. The resulting wet electrodes were transferred to a furnace and annealed in air at 520 °C for 12 h after a ramp rate of 2 °C/min. Annealing times shorter than 12 h resulted in less crystalline films, while annealing longer did not improve crystallinity. The annealing procedure resulted in the formation of ZnO layers on the surface of Fe_2O_3 electrodes and solid-state reactions at the Fe_2O_3/ZnO interface formed $ZnFe_2O_4$ layers around Fe_2O_3 cores. These electrodes were then soaked (while stirring) in 1 M NaOH solution for more than 12 h to remove excess ZnO that did not react with Fe_2O_3.

Surface Modification by Al Treatment. Al^{3+} ions were incorporated into the surface of the $Fe_2O_3/ZnFe_2O_4$ electrodes by introducing 75 μL aqueous solutions of 150 mM $Al(NO_3)_3$ onto the composite electrodes. The resulting wet films were transferred to a furnace and annealed in air at 520 °C for 30 min after a ramp rate of 2 °C/min. The annealing procedure resulted in the formation of Al_2O_3 layers on the $Fe_2O_3/ZnFe_2O_4$ electrodes and by solid state reactions at the interfaces thin $ZnFe_{2-x}Al_xO_4$ and $Fe_{2-x}Al_xO_3$ coating layers were formed on the surface of the composite electrodes. These films were then soaked (while stirring) in 1 M NaOH solution for more than 12 h to remove residual Al_2O_3 on the surface of the $Fe_2O_3/ZnFe_2O_4$ electrodes that were not incorporated into the electrodes.

Adsorption of Co^{2+} Ions As Oxygen Evolution Catalysts. A detailed procedure and explanation for surface modification of Fe_2O_3 electrodes by cobalt ion adsorption can be found elsewhere.[1] Briefly, it involved dipping the electrodes in an aqueous 10 mM $Co(NO_3)_2$ solution for ca. 10 s followed by rinsing the electrodes with approximately 20 mL of DI water, then drying with nitrogen gas. This procedure was repeated twice to ensure complete coverage of the $Fe_2O_3/ZnFe_2O_4$ surface by Co^{2+} ions.

Characterization. Surface morphology of the electrodes was examined using a field emission scanning electron microscope (FEI Nova NanoSEM) operated at 5 kV with a working distance of approximately 5 mm. The electrodes were coated with Pt using a thermal evaporator before imaging to minimize charging problems. Samples were prepared for energy dispersive spectroscopy (EDS) by scraping films off FTO substrates and piling onto carbon tape. Because our films are thinner than the penetration depth of the X-rays used for EDS analysis, this procedure ensures that the majority of the EDS signals is generated by the sample and not by the substrate, which improves the accuracy of the results. EDS analysis was completed using an Oxford Inca system coupled to the FEI Nova NanoSEM. X-ray diffraction patterns were obtained using a Scintag X2 diffractometer (Cu K_α radiation). UV−vis spectra of the films were measured using a Cary 300 UV−vis spectrophotometer in dual-beam transmittance, with bare FTO substrate as a reference.

Electrical and Photoelectrochemical Characterization. Photoelectrochemical measurements were taken with a PAR VMP2 Potentiostat using a three-electrode configuration with the sample as the working electrode, an oversized platinum (1000 Å sputtered on glass, 200 Å Ti adhesion layer) as a counter electrode, and a Ag/AgCl (4 M KCl) reference electrode, again which all further measurements mentioned herein will be referenced. An electrolyte of 1 M NaOH was used in a square, fused-silica beaker. Illumination was provided using a 300 W ozone-free xenon lamp after passing through a water filter and an AM 1.5 (Global) filter. The beam was focused to an optical fiber with the output of the fiber illuminating 0.2 cm^2 of the sample using back-illumination (through FTO substrate), and the incident intensity was adjusted to 100 mW/cm^2 using neutral density filters. Back-illumination was used as it generated higher photocurrent than front-illumination. For Fe_2O_3-based photoanodes with a poor electrical conductivity, using back-illumination that generates electron−hole pairs near the back contact (i.e., FTO substrate) often helps improve photocurrent when the electrode has a porous structure that allows holes to easily reach to the electrode/electrolyte interface.[3,23] Photocurrent measurements were made while linearly sweeping potential from −0.4 V to +0.65 V vs Ag/AgCl with a scan rate of 10 mV/s or while applying a constant potential of +0.4 V vs Ag/AgCl. Capacitance measurements were carried out to obtain Mott−Schottky plots using an EG&G Princeton Applied Research potentiostat/galvanostat model 263A interlinked with a Princeton Applied Research FRD100 frequency response detector using the PowerSine software program. A sinusoidal perturbation of 20 mV was applied at frequency of 10 kHz. The solution and the electrode setup were identical to those used for photocurrent measurement.

Scheme 2. Schematic Representation of a Method Used in This Study to Form a $Fe_2O_3/ZnFe_2O_4$ Electrode; (a) Addition of Zn^{2+}-Containig Solution on Nanoporous Fe_2O_3 Electrode, (b) ZnO layer Formed upon Heating Initiating Solid State Reaction with Fe_2O_3, (c) Formation of $ZnFe_2O_4$ Layers on Fe_2O_3 Particles, and (d) Removal of Excess ZnO

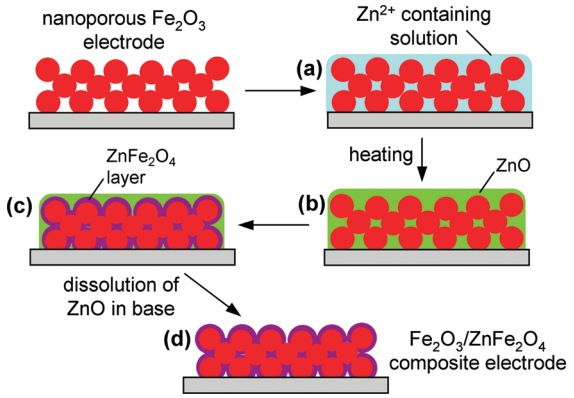

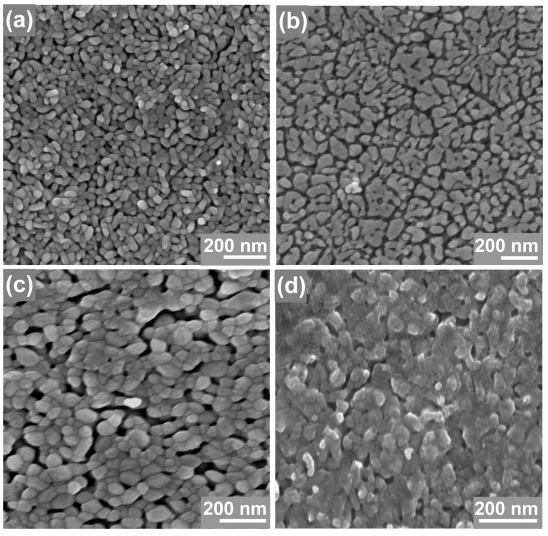

Figure 1. SEM images of (a) untreated Fe_2O_3 electrode, Fe_2O_3 electrodes treated with a 75 μL of 60 mM $Zn(NO_3)_2$ solution (b) before and (c) after removal of residual ZnO, (d) Fe_2O_3 electrode treated with a 75 μL of 60 mM $Zn(NO_3)_2$ solution twice after removal of residual ZnO.

3. RESULTS AND DISCUSSION

The $Fe_2O_3/ZnFe_2O_4$ composite photoanodes were prepared by chemically converting the surface of Fe_2O_3 particles to a $ZnFe_2O_4$ coating layer. The Fe_2O_3 electrode used in this study was produced by anodic electrodeposition of amorphous FeOOH films followed by annealing at 520 °C in the air. The resulting Fe_2O_3 electrodes were composed of 40 - 80 nm round particles, creating a nanoporous network. To the nanoporous Fe_2O_3 electrode, the Zn^{2+} ions were introduced as the form of an aqueous $Zn(NO_3)_2$ solution that can easily penetrate between the Fe_2O_3 nanoparticles and wet the surface (Scheme 2a). When the Fe_2O_3 electrode containing $Zn(NO_3)_2$ solution was annealed at 520 °C, the solution evaporated and the Zn^{2+} ions formed ZnO layers surrounding each Fe_2O_3 particle enabling the

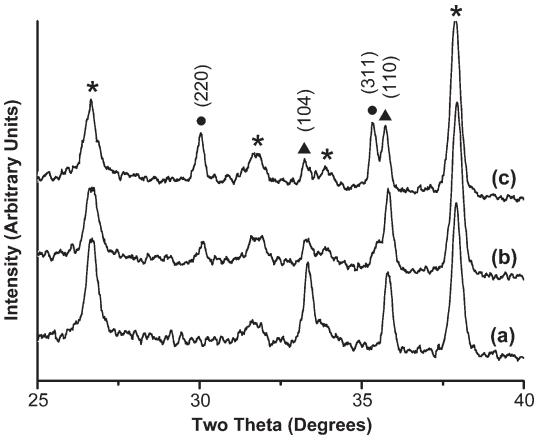

Figure 2. X-ray diffraction spectra of (a) untreated α-Fe_2O_3 electrode and $Fe_2O_3/ZnFe_2O_4$ electrodes obtained by (b) the first and (c) second Zn treatment after the removal of excess ZnO. Diffraction peaks from Fe_2O_3 (▲), $ZnFe_2O_4$ (•), and FTO (*) are indicated.

solid state reaction to occur between the Fe_2O_3 and ZnO to form $ZnFe_2O_4$ (Scheme 2b,c). After the heating procedure, remaining unreacted ZnO was removed by soaking the electrode in a strong alkaline aqueous solution (1 M NaOH) where Fe_2O_3 and $ZnFe_2O_4$ are chemically stable (Scheme 2d).

The amount of $ZnFe_2O_4$ formed on Fe_2O_3 particles could be altered by changing the concentration of $Zn(NO_3)_2$ solutions added to the electrodes or by repeating the procedures (hereafter referred to as Zn-treatment) described in Scheme 2. The SEM image of the bare Fe_2O_3 electrode used in this study is shown in Figure 1a. A Fe_2O_3 electrode treated with 75 μL of 60 mM $Zn(NO_3)_2$ solution after heating 520 °C for 12 h before and after dissolution of excess ZnO formed are also shown in Figure 1b and c. The same electrode after the second Zn-treatment using the identical conditions after the removal of ZnO is shown in Figure 1d. As more of the Fe_2O_3 is converted to $ZnFe_2O_4$ (Figure 1a→1c→1d), the porosity and the overall surface area of the electrode decrease because the incorporation of zinc and oxygen into the Fe_2O_3 particles increases the total volume and the mass of the deposits. Because of the reduction in the surface area accompanied by the conversion of Fe_2O_3 to $ZnFe_2O_4$, converting more of the Fe_2O_3 to $ZnFe_2O_4$ after an optimum amount of $ZnFe_2O_4$ was formed was detrimental for enhancing photocurrent. Our investigation of $Fe_2O_3/ZnFe_2O_4$ electrodes obtained by varying Zn-treatment conditions suggested that the optimum $Fe_2O_3/ZnFe_2O_4$ composition for enhancing photocurrent was obtained when the Zn-treatment was performed twice using 75 μL of 60 mM $Zn(NO_3)_2$ solution, the surface image of which is shown in Figure 1d.

The formation of $ZnFe_2O_4$ in the Zn-treated Fe_2O_3 electrode was confirmed by XRD. Figure 2 shows that as the Zn-treatment was repeated, the intensity of the diffraction peaks originating from $ZnFe_2O_4$ increases while the intensity of the diffraction peaks originating from Fe_2O_3 decreases. The EDS results show that after the first and the second Zn-treatment, the mole ratios of Fe_2O_3:$ZnFe_2O_4$ in the film were 3:1 and 1:1, respectively. (In other words, 25 and 50 mol % of Fe_2O_3 reacted with Zn^{2+} and were converted to $ZnFe_2O_4$ by the first and the second Zn-treatment, respectively.) Since the formation of $ZnFe_2O_4$ initiates on the surface of Fe_2O_3 particles, the resulting $Fe_2O_3/ZnFe_2O_4$ composite electrode is most likely composed of particles with Fe_2O_3 cores and $ZnFe_2O_4$ outer coating layers. UV−vis spectra of

dx.doi.org/10.1021/cm202399g |*Chem. Mater.* 2011, 23, 4863–4869

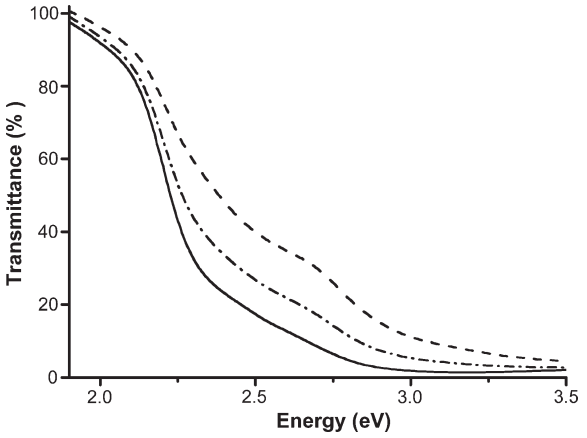

Figure 3. UV−vis spectra of untreated Fe_2O_3 electrode (—) and $Fe_2O_3/ZnFe_2O_4$ electrodes obtained after the first (-··-) and the second Zn-treatment (---).

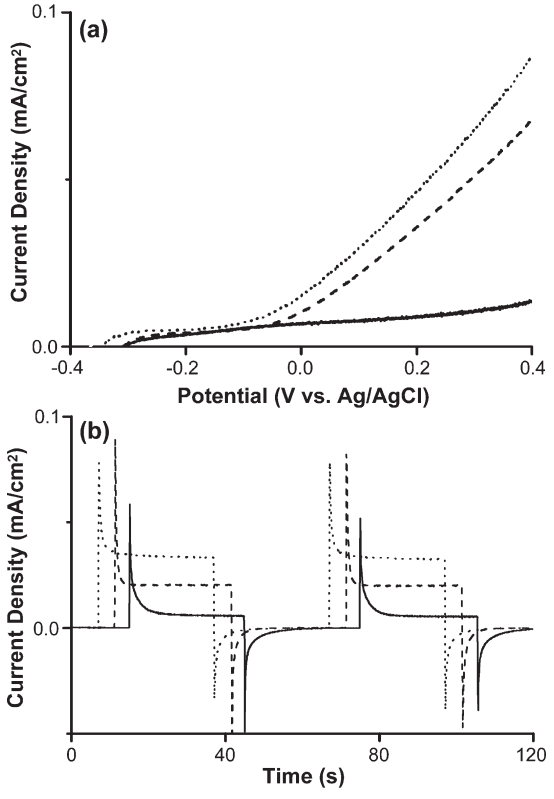

Figure 4. (a) Photocurrent−voltage characteristics and (b) photocurrent measured at +0.4 V vs Ag/AgCl in 1 M NaOH with AM 1.5 G illumination (100 mW/cm^2) of untreated α-Fe_2O_3 (—) and $Fe_2O_3/ZnFe_2O_4$ electrodes obtained after the first (---) and the second Zn-treatment (···). Dark current in $I-V$ measurements is indicated as a gray line in (a).

the Fe_2O_3 and $Fe_2O_3/ZnFe_2O_4$ electrodes show that as the amount of $ZnFe_2O_4$ increases, the amount of light absorbed in the visible region gradually decreases although the absorption onset due to the band gap transition remains at the same position (Figure 3). As no loss of Fe_2O_3 or $ZnFe_2O_4$ occurred during the conversion of Fe_2O_3 to $ZnFe_2O_4$ or during the removal of excess ZnO, this result suggests that the absorption coefficient of $ZnFe_2O_4$ is smaller than that of Fe_2O_3.

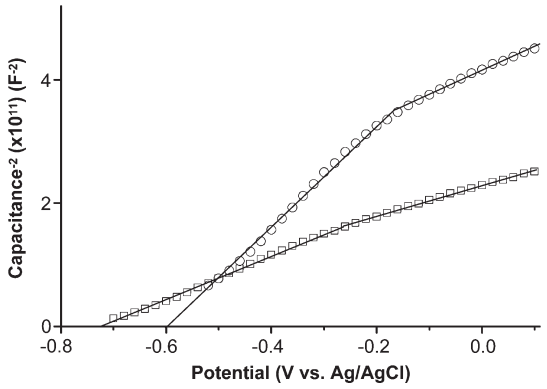

Figure 5. Mott−Schottky plots obtained in 1 M NaOH at 10 kHz of untreated Fe_2O_3 electrode (□) and $Fe_2O_3/ZnFe_2O_4$ electrode obtained after the second Zn-treatment (○).

The photoelectrochemical properties of the native Fe_2O_3 electrode and $Fe_2O_3/ZnFe_2O_4$ composite electrodes were compared by measuring photocurrent in a 1 M NaOH solution while sweeping potential to the positive direction under AM 1.5 illumination (100 mW/cm^2). Figure 4a shows that the photocurrent of the $Fe_2O_3/ZnFe_2O_4$ composite electrodes are considerably enhanced compared to that of the bare Fe_2O_3 electrode and the $Fe_2O_3/ZnFe_2O_4$ electrode obtained after two times Zn-treatment showed the highest photocurrent. The same trend was observed when photocurrent was measured while applying a constant bias of +0.4 V against the reference electrode (Figure 4b). However, when the Zn-treatment is performed three times, photocurrent started to decrease due to the significant reduction of the surface area overriding any favorable effect created by the addition of $ZnFe_2O_4$ layers.

Mott−Schottky plots of the Fe_2O_3 electrode and the $Fe_2O_3/ZnFe_2O_4$ electrode obtained after two times Zn-treatment are shown in Figure 5. The addition of a $ZnFe_2O_4$ layer on the surface of Fe_2O_3 increases the slope near the flat band potential and shifted the flat band potential to the positive direction compared to that of the bare Fe_2O_3 electrode while the slope at potentials above −0.2 V remain similar. Although the Mott−Schottky plots obtained from nanoporous systems may need to be interpreted with caution, this result qualitatively suggests that the observed photocurrent enhancement of the $Fe_2O_3/ZnFe_2O_4$ electrode is not due to a favorable change in charge carrier density or flat band potential. Therefore, it is most likely that the observed photocurrent enhancement of the composite electrode is mainly due to the enhancement in electron−hole separation at the $Fe_2O_3/ZnFe_2O_4$ interface expected from their band edge positions shown in Scheme 1. As explained earlier, a Fe_2O_3 core with a $ZnFe_2O_4$ shell structure can allow the photon generated holes in the Fe_2O_3 core to be transferred to the $ZnFe_2O_4$ layer and then consumed at the $ZnFe_2O_4$/electrolyte junction. This can effectively increase photon to photocurrent conversion ratio of Fe_2O_3 that has an extremely short hole diffusion length.[21,22] The photon generated electrons in the $ZnFe_2O_4$ layer can be transferred to the Fe_2O_3 core and move to the back contact. Considering that the total photon absorption of the composite electrode is less than that of the bare Fe_2O_3 electrode (Figure 3), the enhanced photocurrent generated by the composite electrode indicates that the photocurrent gain by the reduced electron−hole recombination is considerable.

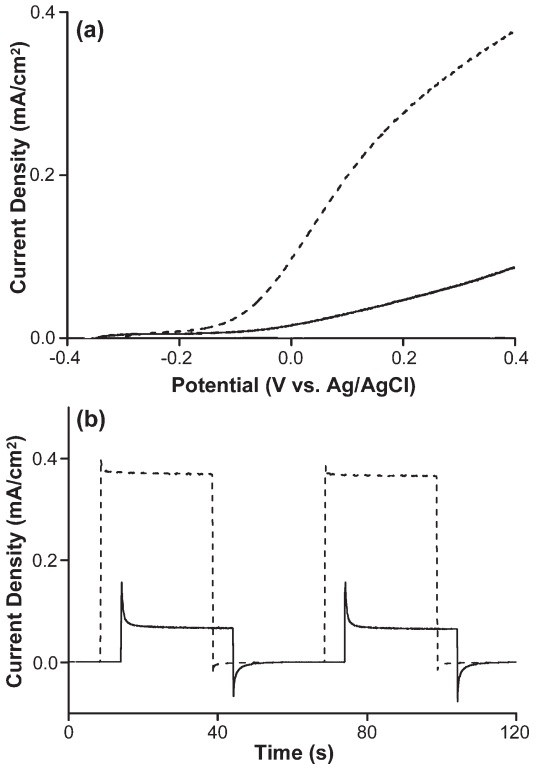

Figure 6. (a) Photocurrent−voltage characteristics and (b) photocurrent measured at +0.4 V vs Ag/AgCl in 1 M NaOH with AM 1.5 G illumination (100 mW/cm^2) of Fe_2O_3/$ZnFe_2O_4$ electrodes before (—) and after (---) Al-treatment. Dark current in $I-V$ measurements is indicated as a gray line in (a).

To further enhance the photocurrent of the Fe_2O_3/$ZnFe_2O_4$ electrode, we treated the surface of the Fe_2O_3/$ZnFe_2O_4$ electrode with $Al(NO_3)_3$ solution using the same procedure used for the formation of $ZnFe_2O_4$ layer (Scheme 1). Previously, we have demonstrated that surface modification of Fe_2O_3 with Al^{3+} ions to form a thin $Fe_2O_3-Al_2O_3$ solid solution layer on the surface of the Fe_2O_3 electrode can effectively reduce the surface states created by the Fe^{3+} ions exposed at the surface with imperfect coordination.[3] Since Al_2O_3 and Fe_2O_3 are isostructural, $Fe_2O_3-Al_2O_3$ solid solution layers can easily form on the Fe_2O_3 surface and Fe^{3+} ions in the solid solution layer can have a local environment that is similar to those in the bulk crystal Fe_2O_3 structure. As a result, formation of a thin $Fe_2O_3-Al_2O_3$ solid-solution layer on the surface of the Fe_2O_3 electrode can effectively minimize Fe^{3+} ions exposed at the surface with imperfect coordination environments and, therefore, the surface states located in the band gap region that can serve as recombination centers.

We postulated that Al treatment on the Fe_2O_3/$ZnFe_2O_4$ electrode may have a similar effect if Al_2O_3 forms a thin surface solid solution layer with $ZnFe_2O_4$ ($ZnFe_{2-x}Al_xO_4$) or with Fe_2O_3 ($Fe_{2-x}Al_xO_3$) that was not completely covered by $ZnFe_2O_4$.[24,25] For the Al-treatment, 75 μL of 20 mM $Al(NO_3)_3$ solution was used and the heat treatment was performed at 520 °C. After the heat treatment, excess Al_2O_3 that did not form the solid solution layer with $ZnFe_2O_4$ or Fe_2O_3 was removed by 1 M NaOH.

An SEM image of the Al-treated Fe_2O_3/$ZnFe_2O_4$ electrode after the removal of unreacted Al_2O_3 is shown in the Supporting Information (Figure S1). The surface of the film became roughened indicating the incorporation of Al altering the surface composition.

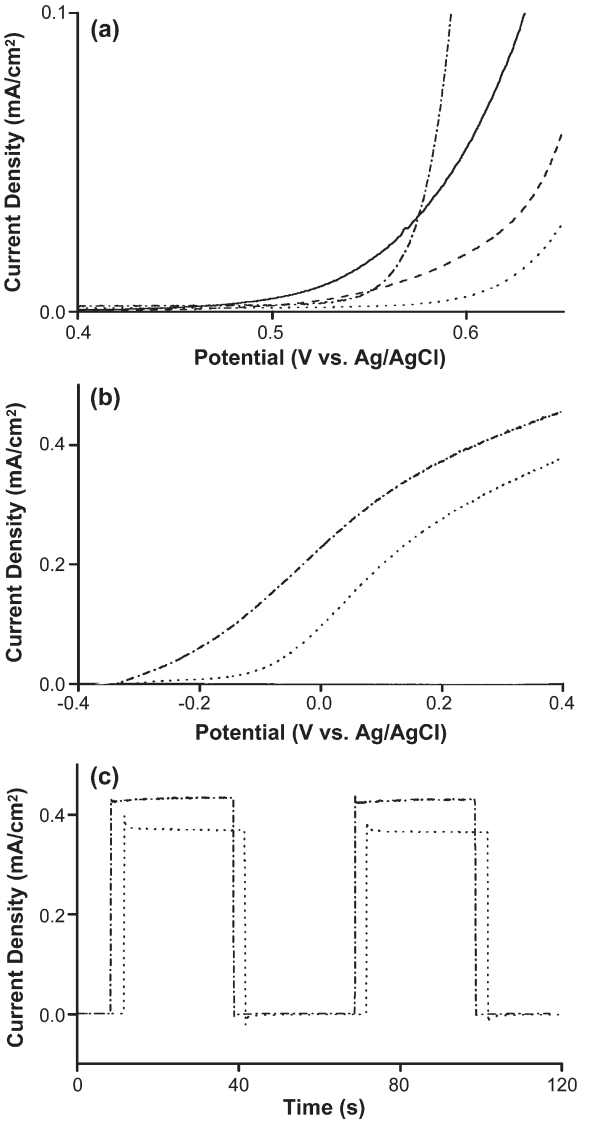

Figure 7. (a) $I-V$ characteristics of Fe_2O_3 (—), Fe_2O_3/$ZnFe_2O_4$ (---), Al-treated Fe_2O_3/$ZnFe_2O_4$ (···), Al-treated Fe_2O_3/$ZnFe_2O_4$ after Co^{2+} adsorption (-··) showing the onset of electrochemical O_2 evolution in the dark in 1 M NaOH. (b) Photocurrent−voltage characteristics and (c) photocurrent measured at +0.4 V vs Ag/AgCl in 1 M NaOH with AM 1.5 G illumination (100 mW/cm^2) of Al-treated Fe_2O_3/$ZnFe_2O_4$ electrode before (···) and after (-··) Co^{2+} adsorption. Dark scan in I−V measurements is indicated as a gray line.

EDS analysis of an Al-treated Fe_2O_3/$ZnFe_2O_4$ electrode shows that the amount of Al incorporated is 3.5 at % of the total cationic sites in the composite electrode (= mol(Al)/mol(Al + Zn + Fe) × 100). Because the amount of Al incorporated to the film is not significant, the XRD pattern of the Al-treated sample did not show any noticeable change from that of the Fe_2O_3/$ZnFe_2O_4$ electrode before Al treatment (see the Supporting Information, Figure S2).

Photocurrent measurements, however, show that the subtle incorporation of Al into the Fe_2O_3/$ZnFe_2O_4$ surface caused a considerable increase in photocurrents obtained both with sweeping potential (Figure 6a) and at a constant bias (Figure 6b). In particular, photocurrent measured at a constant bias of +0.4 V shows that the presence of Al significantly decreased the transient

dx.doi.org/10.1021/cm202399g |*Chem. Mater.* 2011, 23, 4863–4869

photocurrent after light is turned on and off. This reduction in transient photocurrent is indicative of a decrease in surface charge recombination, which is most likely due to the reduction of surface states.[3,26,27] Comparison of the Mott−Schottky plots for Fe_2O_3/$ZnFe_2O_4$ electrodes before and after Al-treatment did not show any significant change for both the slope and the flat band potential, confirming that the observed photocurrent enhancement is not due to Al^{3+} ions altering the carrier density or flat band potential of the Fe_2O_3/$ZnFe_2O_4$ electrodes (see the Supporting Information, Figure S3).[3]

The reduction of the transient photocurrent can also be resulted if the surface of the semiconductor electrode becomes more catalytic for the reaction involving interfacial charge transfer processes, which will also decrease surface recombination. In order to check for the possibility of the Al-treatment causing the surface of the Fe_2O_3/$ZnFe_2O_4$ electrode to be more catalytic for O_2 evolution, the $I-V$ characteristics of Fe_2O_3/$ZnFe_2O_4$ composite electrodes before and after Al-treatment as well as bare Fe_2O_3 electrode were measured in the dark while the potential was swept to the positive direction to induce electrochemical oxidation of water to O_2 (Figure 7a). For typical single-crystal n-type electrodes that develop a high-quality depletion layer with upward band bending at the electrode/electrolyte junction, electrochemical oxidation of water is not observed in the dark as the external bias necessary to oxidize water signifies the band bending (i.e., reverse bias condition) and prevents the flow of anodic current to the semiconductor electrode. However, for nanoporous electrodes that do not develop well-defined band bending at the interface and possess numerous surface states located near the water oxidation potential, electrochemical oxidation of water can often be observed in the dark when an appropriate amount of external bias is applied. In this case, the electrical onset potential of O_2 evolution can be used to compare the catalytic nature of the semiconductor electrodes for O_2 evolution if the electrodes compared to each other have comparable conductivities, thickness, and morphologies (particle sizes, particle connectivities, and surface areas), with the only difference being the surface composition or nature.

Figure 7a shows that the onset of O_2 evolution on the Fe_2O_3/$ZnFe_2O_4$ electrode is shifted to the positive direction compared to that of the native Fe_2O_3 electrode. It also shows that Al-treatment made the surface of Fe_2O_3/$ZnFe_2O_4$ electrode even less catalytic for O_2 evolution and caused an additional 50 mV shift of the onset potential to the positive direction. This result confirms that the reduction of transient current and the enhancement of photocurrent caused by the Al-treatment is not due to the surface becoming more catalytic, which supports our claim that the main effect of the Al-treatment is the reduction of surface states.

The fact that the Al-treated sample showed a significant photocurrent enhancement although it made the surface less catalytic for O_2 evolution also suggests that when an O_2 evolution catalyst is introduced to the surface, the photocurrent generated by the Al-treated Fe_2O_3/$ZnFe_2O_4$ may be further enhanced. We tested this possibility by adsorbing Co^{2+} ions to the Al-treated Fe_2O_3/$ZnFe_2O_4$ surface. Previous studies have shown the Co^{2+} ions adsorbed on to the surface of Fe_2O_3 can act as a simple yet efficient oxygen evolution catalyst.[1,3] Therefore, we postulated that Co^{2+} ions could also act as a catalyst on an Al-treated $ZnFe_2O_4$/Fe_2O_3 electrode considering the similarities of Fe_2O_3 and Fe_2O_3/$ZnFe_2O_4$ electrodes.

Figure 7a shows that when Co^{2+} ions were adsorbed to the Al-treated Fe_2O_3/$ZnFe_2O_4$ surface, it clearly enhanced the electrochemical oxidation of water to O_2 in the dark, confirming the catalytic ability of Co^{2+} ions adsorbed on the Fe_2O_3/$ZnFe_2O_4$ electrode. The effect of Co^{2+} ions was also evident in photocurrent−potential characteristics shown in Figure 7b where the photocurrent onset is shifted to the negative direction and the overall photocurrent is enhanced significantly. When the photocurrent was measured at a constant bias of +0.4 V, the presence of Co^{2+} ions completely removed the presence of transient photocurrent and improved the steady state photocurrent by 18% (Figure 7c).

4. CONCLUSIONS

We have prepared α-Fe_2O_3/$ZnFe_2O_4$ composite photoelectrodes using a simple surface treatment on nanoparticulate α-Fe_2O_3 electrodes to improve its overall photoelectrochemical performance. The conversion of α-Fe_2O_3 to $ZnFe_2O_4$ was limited to only the surface of Fe_2O_3 particles by the mild heating condition, resulting in the formation of composite films composed of particles with a Fe_2O_3 core and a $ZnFe_2O_4$ shell. The composite electrode generating the highest photocurrent contained 1:1 mol ratio of Fe_2O_3 and $ZnFe_2O_4$. When more Fe_2O_3 was converted to $ZnFe_2O_4$, the accompanying mass and volume increase of the electrode resulted in the significant reduction of the surface area and the net effect was not favorable in increasing photocurrent. $I-V$ characteristics in the dark and the Mott−Schottky plots of the bare Fe_2O_3 and Fe_2O_3/$ZnFe_2O_4$ electrodes indicated that the enhanced photocurrent observed by the Fe_2O_3/$ZnFe_2O_4$ composite electrode is not due to the improved O_2 evolution kinetics, favorable changes in the doping level, or in the position of flat band potential. Therefore, it was concluded that the photocurrent increase is mainly due to the enhanced electron−hole separation at the Fe_2O_3/$ZnFe_2O_4$ interface. Further enhancement in photocurrent was obtained through the Al-treatments of the composite electrodes, which can form thin solid solution coating layers (i.e., $ZnFe_{2-x}Al_xO_4$ or $Fe_{2-x}Al_xO_3$) and reduce surface states that can serve as the electron−hole recombination centers. The $I-V$ characteristics in the dark near the electrochemical onset of O_2 evolution shows that both the formation of $ZnFe_2O_4$ layer and incorporation of Al^{3+} ions on the surface made the surface less catalytic for oxygen evolution. When Co^{2+} ions were introduced to the surface of composite electrodes as oxygen evolution catalysts, the onset of photocurrent was shifted to the negative direction by ca. 50 mV and the overall photocurrent was also improved. The simple solution/heat treatment used in this study may be used to convert various binary oxide nanoparticulate electrodes to electrodes containing more complex ternary compositions and/or to tune surface compositions to improve the overall photoelectrochemical performances.

■ ASSOCIATED CONTENT

Supporting Information. SEM images, XRD patterns, and Mott−Schottky plots of Fe_2O_3/$ZnFe_2O_4$ electrodes before and after Al treatment. This information is available free of charge via the Internet at http://pubs.acs.org.

■ AUTHOR INFORMATION

Corresponding Author

*E-mail: kchoi1@purdue.edu. Tel: 1-765-494-0049. Fax: 1-765-494-0239.

■ ACKNOWLEDGMENT

This work was supported by the Division of Chemical Sciences, Geosciences, and Biosciences, Office of Basic Energy Sciences of the U.S. Department of Energy through Grant DE-FG02-05ER15752 and made use of the Life Science Microscopy Facility at Purdue University.

■ REFERENCES

(1) Kay, A.; Cesar, I.; Gratzel, M. *J. Am. Chem. Soc.* **2006**, *128*, 15714-15721 and references therein.
(2) Spray, R. L.; Choi, K. S. *Chem. Mater.* **2009**, *21*, 3701–3709.
(3) Spray, R. L.; McDonald, K. J.; Choi, K. S. *J. Phys. Chem. C.* **2011**, *115*, 3497–3506.
(4) Dehaart, L. G. J.; Blasse, G. *Solid State Ionics* **1985**, *16*, 137–139.
(5) Tahir, A. A.; Wijayantha, K. G. U.; Mazhar, M.; McKee, V. *Thin Solid Films* **2010**, *518*, 3664–3668.
(6) Matsumoto, Y. *J. Phys. Chem.* **1996**, *126*, 227–234.
(7) Ida, S.; Yamada, K.; Matsunaga, T.; Hagiwara, H.; Matsumoto, Y.; Ishihara, T. *J. Am. Chem. Soc.* **2011**, *132*, 17343–17345.
(8) Kim, H. G.; Borse, P. H.; Jang, J. S.; Jeong, E. D.; Jung, O. S.; Suh, Y. J.; Lee, J. S. *Chem. Commun.* **2009**, *39*, 5889–5891.
(9) Shifu, C.; Wei, Z.; Wei, L.; Huaye, Z.; Xiaoling, Y.; Yinghao, C. *J. Hazard. Mater.* **2009**, *172*, 1415–1423.
(10) Liu, Z. F.; Zhao, Z. G.; Miyauchi, M. *J. Phys. Chem. C.* **2009**, *113*, 17132–17137.
(11) Liu, Z. F.; Miyauchi, M. *Chem. Commun.* **2009**, *15*, 2002–2004.
(12) Matsumoto, Y.; Omae, M.; Sugiyama, K.; Sato, E. *J. Phys. Chem.* **1987**, *91*, 577–581.
(13) Cao, X. B.; Gu, L.; Lan, X. M.; Zhao, C.; Yao, D.; Sheng, W. J. *Mater. Chem. Phys.* **2007**, *106*, 175–180.
(14) Cheng, P.; Li, W.; Zhou, T.; Jin, Y.; Gu, M. *J. Photochem. Photobiol., A* **2004**, *168*, 97–101.
(15) Yuan, Z. H.; Zhang, L. D. *J. Mater. Chem.* **2001**, *11*, 1265–1268.
(16) Bai, J. *Mater. Lett.* **2009**, *63*, 1485–1488.
(17) Valenzuela, M. A.; Bosch, P.; Jimenez-Becerrill, J.; Quiroz, O.; Paez, A. I. *J. Photochem. Photobiol., A* **2002**, *148*, 177–182.
(18) Peng, T. Y.; Lv, H. J.; Ma, L.; Zeng, P.; Ke, D. N. *J. Mater. Chem.* **2010**, *20*, 3665–3672.
(19) Yin, J.; Bie, L.-J.; Yuan, Z.-H. *Mater. Res. Bull.* **2007**, *42*, 1402–1406.
(20) Hou, Y.; Li, X. Y.; Zhao, Q. D.; Quan, X.; Chen, G. H. *Adv. Funct. Mater.* **2010**, *20*, 2165–2174.
(21) Dare-Edwards, M. P.; Goodenough, J. B.; Hamnett, A.; Trevellick, P. R. *J. Chem. Soc., Faraday Trans.* **1983**, *1*, 2027–2041.
(22) Kennedy, J. H.; Frese, K. W. *J. Electrochem. Soc.* **1978**, *125*, 709–714.
(23) Bjorksten, U.; Moser, J.; Gratzel, M. *Chem. Mater.* **1994**, *6*, 858–863.
(24) Toledo, J. A.; Valenzuela, M. A.; Bosch, P.; Armendáriz, H.; Montoya, A.; Nava, N.; Vázquez, A. *Appl. Catal., A* **2000**, *198*, 235–245.
(25) Toledo, J. A.; Bosch, P.; Valenzuela, M. A.; Montoya, A.; Nava, N. *J. Mol. Catal. A: Chem.* **1997**, *125*, 53–62.
(26) Le Formal, F.; Tetreault, N.; Cornuz, M.; Moehl, T.; Gratzel, M.; Sivula, K. *Chem. Sci.* **2011**, *2*, 737–743.
(27) Hisatomi, T.; Le Formal, F.; Cornuz, M.; Brillet, J.; Tetreault, N.; Sivula, K.; Gratzel, M. *Energy Environ. Sci.* **2011**, *4*, 2512–2515.